Microelectronics Reliability 99 (2019) 113–118

Contents lists available at ScienceDirect

Microelectronics Reliability

journal homepage: www.elsevier.com/locate/microrel

Degradation of AlInAs/InGaAs/InP quantum cascade lasers due to electrode adhesion failure

D. Pierścińska*, K. Pierściński, G. Sobczak, P. Gutowski, M. Płuska, M. Bugajski

Institute of Electron Technology, Al. Lotników 32/46, 02-668 Warsaw, Poland

ARTICLE INFO

Keywords:
Quantum cascade laser
Thermoreflectance spectroscopy
Degradation mechanisms
Electrode adhesion

ABSTRACT

In this paper external degradation type of failure of Quantum Cascade Laser is analyzed. The failure mode discussed in the work is connected with the damage of the gold, top electrode. We show how fabrication faults translate to degradation of device and monitor temperature distributions as well as electrical characteristics of the device during the process.

The aim of this research is to demonstrate how external degradation process develops in case of AlInAs/InGaAs/InP quantum cascade lasers.

1. Introduction

Studies of degradation mechanisms of semiconductor lasers based on the GaAs family of materials have been performed from mid 1960s [1–3] beginning with those concerning GaAs homojunction laser diodes. After the development of heterostructure lasers and the achievement of CW operation at room temperature (early 1970s), the problem of degradation of semiconductor lasers became apparent. Reliability of many kinds of semiconductor devices has been greatly improving for about 50 years. Throughout this period, various degradation mechanisms have been discovered leading to increased understanding of processes occurring in devices and consequently improving reliability.

This paper focuses on the degradation mechanism present in quantum cascade lasers (QCLs)-type of semiconductor lasers based on intersubband transitions. QCLs were demonstrated for the first time in 1994 in Bell Labs by group of prof. F. Capasso [4]. Since then, QCLs underwent a rapid development. Despite significant improvement of parameters of devices [5–7] and optimization of their construction [8,9], reliability and device lifetime are still two critical parameters of the QCLs, deciding about further development and limiting their applications. Currently, the knowledge about processes responsible for degradation of quantum cascade lasers is still limited; there are not many papers published dealing with this problem from experimental point of view [10–12]. The common belief, although not fully experimentally confirmed, is that QCLs are more reliable devices compared to interband edge emitters. This is based on the fact that in case of intersubband semiconductor lasers there is no reabsorption of emitted radiation at the laser facets, which is one of the main causes for interband edge-emitters failure [13,14]. The process of reabsorption leads to the local overheating of facets beyond the temperature of melting point of semiconductor material, which in turn results in catastrophic optical mirror damage (COMD), i.e., irreversible damage of device [15].

Thermal processes in QCL results from large electrical power density required for their operation and low thermal conductivity of complex, multilayer heterostructure. Those factors lead to strong local heating inside the device, resulting in significant overheating of active region [16]. High overall temperature of laser core causes a leakage of electrons from the upper laser level into delocalized continuum states and backfilling of the lower laser level by electrons from the subsequent injector. Both effects decrease the population inversion. These are the main limiting factors of high temperature operation of the devices.

Our previous papers [17–19] on degradation problems in QCLs concerned internal degradation mechanisms resulting from overheating of the active area, due to operation conditions (high current and high voltage). Internal degradation usually takes place in the active region and is accelerated by strain, temperature and injection current. However, degradation was observed in various batches of devices, that could not be regarded as internal, and seemed to appear randomly. Careful investigation of several batches of devices, revealed the pattern, that connected the failure of devices to fabrication steps, namely to the dielectric and gold deposition. The work has shown that both technological processes are critical for stable, reliable device and increasing the yield.

In this paper we present results of examination of external degradation mode of QCL. External degradation can occur in different

* Corresponding author.
E-mail address: dorota.pierscinska@ite.waw.pl (D. Pierścińska).

https://doi.org/10.1016/j.microrel.2019.06.003
Received 10 November 2018; Received in revised form 15 May 2019; Accepted 4 June 2019

Table 1
The layer sequence of lattice matched $Al_{0.48}In_{0.52}As/In_{0.53}Ga_{0.47}As/InP$ QCL structure.

		Thickness	Material	Doping
MOVPE	Upper waveguide	500 nm	InP	n = 8e18 cm^{-3}
		1.5 μm	InP	n = 1e17 cm^{-3}
		1.5 μm	InP	n = 4e16 cm^{-3}
MBE		500 nm	InGaAs	n = 4e16 cm^{-3}
	Active region	50 x AlInAs/InGaAs		
	Lower waveguide	500 nm	InGaAs	n = 4e16 cm^{-3}
	Substrate	500 μm	InP	n = 2e17 cm^{-3}

parts of the device: mirror, electrodes, heatsink, bonding, metal coating of the heatsink. This work presents impact of electrode adhesion failure on electrical and thermal parameters and in the end on the degradation of mid-IR, InP-based QCL.

2. Investigated devices

The study of degradation mode was performed for lattice matched AlInAs/InGaAs/InP QCL grown by combined MBE and MOVPE. It was designed for emission at about 9.2 μm. Growth of the active region was performed by solid source MBE on Riber Compact 21T reactor [20]. MOVPE overgrowth was performed using AIXTRON 3 × 2″ FT LP-MOVPE system with vertical, shower-head reactor. The AlInAs/InGaAs active region of the laser was grown on lightly doped ($n = 2 \times 10^{17}$ cm^{-3}) InP substrate serving as a lower waveguide. The InP top waveguide consisted of 1.5 μm, $n = 4 \times 10^{16}$ cm^{-3} layer followed by 1.5 μm, $n = 1 \times 10^{17}$ cm^{-3} layer. The whole structure was completed by highly doped ($n = 8 \times 10^{18}$ cm^{-3}) contact layer. The details of layer structure of the laser are listed in the Table 1 [20].

The epitaxial wafers were processed in a standard double trench (DT) design with wet etching of trenches. Si_3N_4 was used to provide electrical isolation. For current injection, 15 μm wide window was opened in the insulator. Laser chips, 2 mm long, were soldered epi-side up to Au-plated AlN submount, and then to cooper heatsinks using indium solder. Details of the processing technology are given in our earlier papers concerning InP-based QCLs [21]. In this paper uncoated devices were investigated.

3. Experimental results

To perform complex analysis of degradation of investigated AlInAs/InGaAs/InP QCLs, complementary experimental techniques were applied. To determine electrooptical parameters and their evolution during degradation process Light-Current-Voltage (LIV) curves were registered [22]. Analysis of thermal processes occurring at the laser facet: localization of the heat sources and defects on the facets, identification of heat propagation directions was achieved by performing thermoreflectance (TR) measurements [23,24]. To gain insight into microscopic failure mechanisms of QCLs, the degraded lasers were analyzed by means of focused ion beam (FIB) and scanning electron microscope (SEM) techniques with energy dispersive spectroscopy (EDS) analysis. Additionally, the devices were inspected by means of optical microscopy, which allow observation of external damage to device at the facets, solder, heatsink and electrodes.

First part of investigation included performing electrooptical characterization and visual inspection of the investigated devices. Fig. 1(a) shows comparison of LIV measurements for investigated laser chip before and after mounting to AlN and copper heatsink. For reference purposes, Fig. 1(a) contains LIV characteristic of mounted chip from the same batch, registered under the same experimental conditions (grey line). Compared to reference device, the investigated chip exhibits additional current path, what manifests in increased threshold current value.

In LIV data we observed increase of the threshold current of investigated device after mounting process. The value of threshold current increased by factor 2 from 1.26 A to 2.5 A while maintaining almost the same threshold voltage at the level ~11.5 V. This behaviour of the device suggests creating an additional path for the current flow. Optical inspection with microscope, presented in Fig. 1(b), revealed area at front facet, where the gold from the electrode seems to shorten the device by touching the facet at the position of AR layers, what is even better visible in SEM image presented in Fig. 2(c). Such features were frequently observed in batches of devices, in which we have also identified problems with either dielectric deposition or metal deposition, or usually both.

Investigation of thermal properties of the laser was performed by CCD-thermoreflectance spectroscopy (CCD-TR) [25]. Fig. 2(a–f) presents temperature distribution maps covering the region around active area on the front facet of investigated QCL, covering the region around active area. Maps were registered for the same experimental conditions: pulse width of 10 μs, frequency 20 kHz, heat sink temperature of 20 °C and for different driving currents in the range from 0.3 A to 1.5 A. Maps in the upper row are intentionally presented in different temperature range than maps in the lower row, to enhance the information about AR temperature.

For the first two maps (Fig. 2(a) and (b)) which were registered at 0.3 A and 0.5 A, maximal temperature increase is not localized in the active area but on the area of the gold overlapping on the epitaxial layers. Increase of temperature reaches 240 K for driving current of 0.5 A. Such results confirm, that gold overlapping on the epitaxial layers created additional current path and were the reason of observed overheating in this area and also caused increase of the threshold current for the laser (Fig. 1(a)). For larger driving current of 0.7 A, increase of temperature occurs only in the active area region. That suggests that additional current path was interrupted, most probably the burn-out took place, resulting in formation of isolation layer beneath gold. It is worth noticing, that in map Fig. 2(c), the shape of the feature (gold overlapping on facet) has changed, covering the area of AR of the device. Maps registered for driving currents of 1.1 A, 1.3 A and 1.5 A (Fig. 2(d)–(f)), present temperature distribution shape and temperature increase in the active area, which typical for this type of InP-based QCLs (compare [26]).

The vertical line scans for selected maps are presented in Fig. 3(a) and maximal temperature increases in AR extracted from all registered maps are presented in Fig. 3(b).

Black and blue lines in Fig. 3(a) presents temperature data for line scans taken at the point *A* - center of the active area. The green and red lines present line scans taken at the point *B* - point located on the facet in the vicinity of the overlapping gold. For area of gold overlapping on the laser facet, high temperature increases are registered: for 0.3 A–120 K, for 0.5 A–246 K. These are much higher values than those registered for the active area, and are the result of high current density which flows in this spot. The size of the tip of gold overlap was estimated to be of about 6 μm. Additionally, such parasitic current path has high resistance due to low quality gold to heterostructure electrical contact.

The maximal temperature increases (ΔT) presented in the Fig. 3(b), show that temperature rises very fast in the area of defect and goes to zero abruptly for the next current step. The temperature rise in the active area reaches ~90 K for current of 1.5 A. The LIV curve registered after the TR measurement at 0.7 A shows that the threshold current decreased to the value registered before mounting, i.e. to 1.25 A (threshold voltage remained unchanged), which confirms that parasite electrical path has been destroyed by burn-out.

Further thermal measurements were carried out for higher thermal load, resulting from driving the device with longer current pulses of 20 μs. Fig. 4(a–c) presents temperature distribution maps on front facet of investigated QCL, registered for the same experimental conditions: pulse width of 20 μs, frequency 20 kHz, heat sink temperature of 20 °C

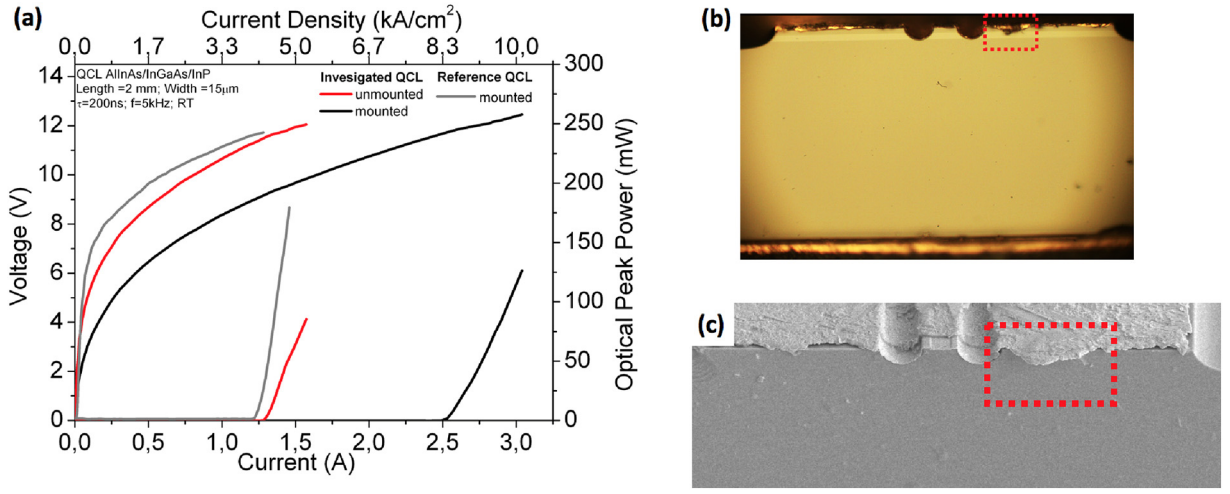

Fig. 1. (a) LIV characteristics for investigated and reference QCLs. Red line corresponds to data for QCL laser chip before mounting, black line - after mounting. Grey lines were registered for reference device from the same batch. The data is collected in pulse mode using 200 ns current pulses and 5 kHz repetition rate at room temperature (RT). (b) Optical microscopy image and (c) SEM image showing front facet of the laser with an area where gold overlaps on epitaxial layers. (For interpretation of the references to color in this figure legend, the reader is referred to the web version of this article.)

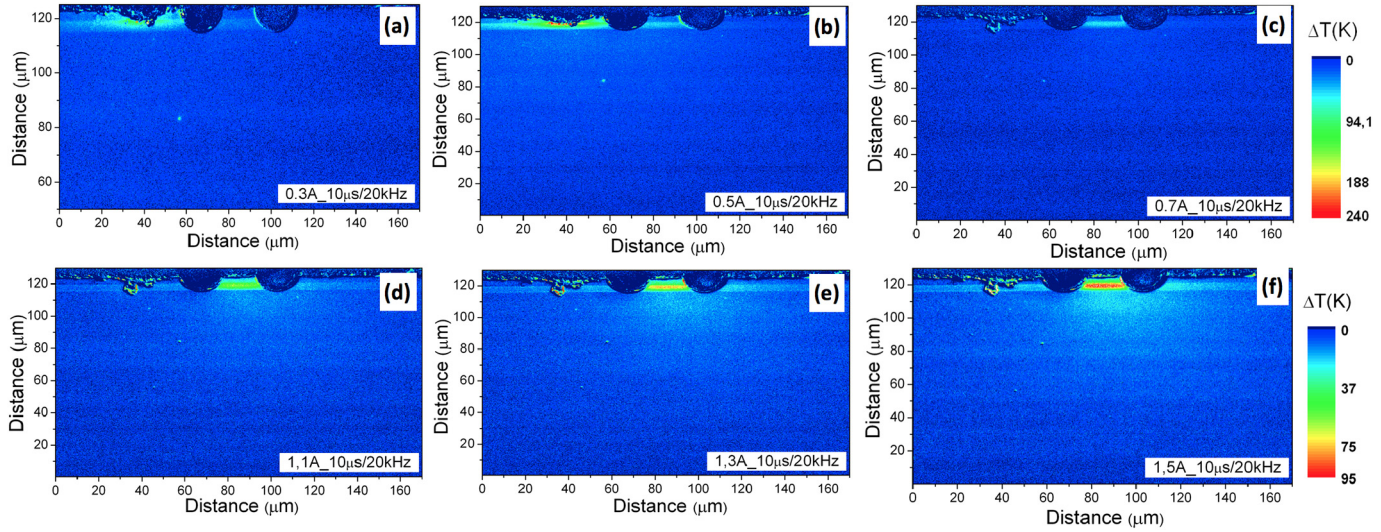

Fig. 2. Temperature distribution maps on the front facet of AlInAs/InGaAs/InP QCLs, measured for pulse width 10 μs and frequency 20 kHz for different driving currents change in the range 0.3 A–1.5 A. Maps are intentionally presented in different temperature ranges to enhance the features.

and different driving currents in the range from 0.3 A to 1.5 A. Fig. 4(d) presents the maximal temperature increases (ΔT) and Fig. 4(e) vertical temperature scans taken at the center of the active area.

Even for low driving current (0.3 A), non-uniform temperature distribution in the active area of the QCL can be observed, with spots exhibiting higher temperature. With the increase of current up to 1.5 A these features are becoming more pronounced. For current of 1.6 A, the laser stopped working – electrical resistance of the device dropped to 2 Ω, no heating is observed (Fig. 4(d)).

Visual inspection performed by optical microscope (Fig. 5) shows damaged areas at different parts of the device. Top view of device presented in Fig. 5(a), shows the electroplated gold layer. Destruction of the metal layers is clearly visible, reaching deep into the semiconductor structure. Fig. 5(b) presents the image of the front facet of the device. The part of mirror with AR and overlapping gold is zoomed into in the inset. In the AR, overheating patterns are clearly visible, indicating high local temperature rise, leading to local melting taking place in the region where the metal migrated on the front facet of the laser. The mirror was clear before the measurements were taken, clearly indicating that features were formed during the degradation of the device.

To investigate in more details the failure of the QCL, degraded laser was analyzed by means of SEM imaging, FIB milling and also by EDS analysis.

Fig. 6(a) presents SEM image of the degraded device. Several FIB cuts were performed perpendicular to the layers at multiple locations along the laser ridge near of the area, starting at the region where large destruction of metal layers was visible in the top view of device. The dashed lines indicate places, where FIB cuts were performed. Fig. 6(b–e) present SEM images for successive FIB cuts. All images of planes revealed by the cuts in the region of interest show problem with gold adhesion, as well as severe melting taking place in the AR layers and top waveguiding layer of the semiconductor structure (Fig. 6(c–e)).

Images shown in Fig. 6, present damage and voids in the area of the interface between semiconductor QCL laser chip and gold layer. It can be observed, that problem with adherence of gold layer consequently leads to damage occurring in the active region of the laser. FIB cuts were performed further along the ridge, away from the damaged area, showing no further damages in active region.

EDS analysis confirms that droplets visible in the active are consist

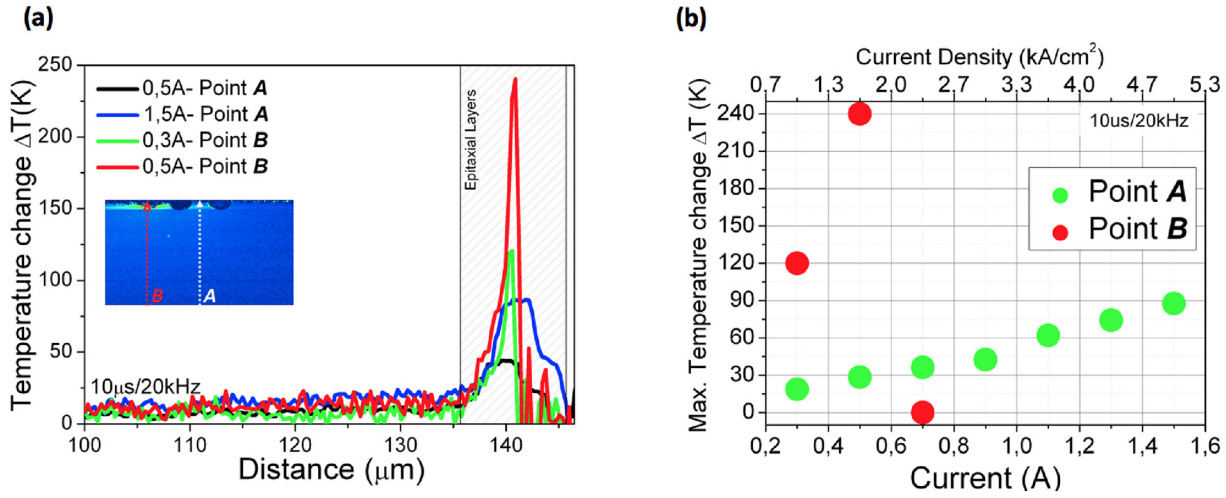

Fig. 3. (a) Temperature distribution line scans across the laser facet, taken at the center of the active area (Point A) and at the area of gold overhanging (Point B) perpendicular to the epitaxial layers. Inset presents a TR map with marked cross-section locations. (b) Maximum temperature increase as a function of driving current. (For interpretation of the references to color in this figure legend, the reader is referred to the web version of this article.)

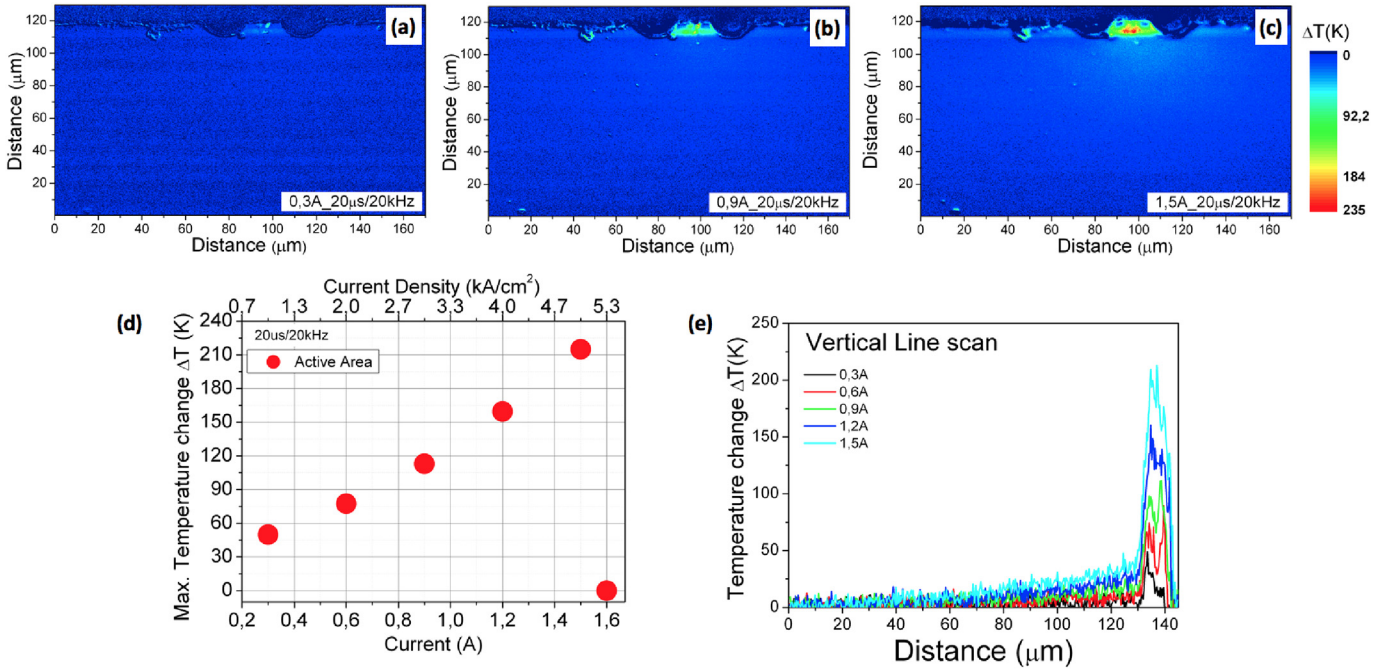

Fig. 4. (a–c) Temperature distribution maps on the front facet of AlInAs/InGaAs/InP QCLs, measured for pulse width 10 µs and frequency 20 kHz for different driving currents change in the range 0,3 A–1,5 A. (d) Maximum temperature increase as a function of driving current. (e) Temperature distribution line scans across the laser facet, taken at the center of the active area perpendicular to the epitaxial layers.

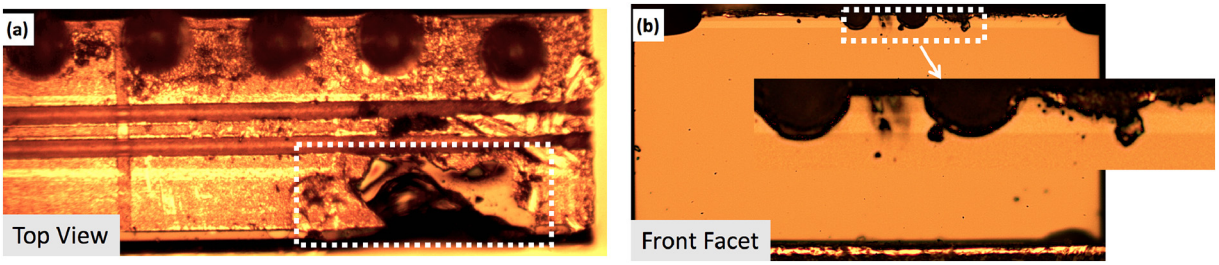

Fig. 5. Optical microscopy images showing top view of the laser chip(a) and front facet of the laser. The frames show areas that have been degraded.

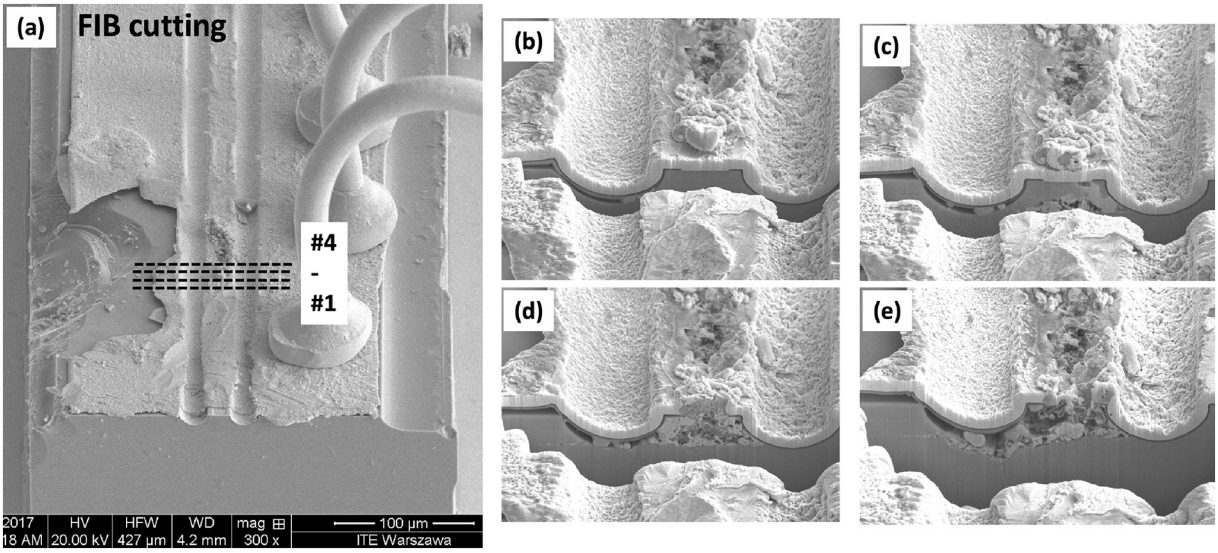

Fig. 6. SEM images of part of the top of the diode laser under test after failure. (a) Locations of cross-sections done by FIB, (b)–(e) SEM images of cross sections.

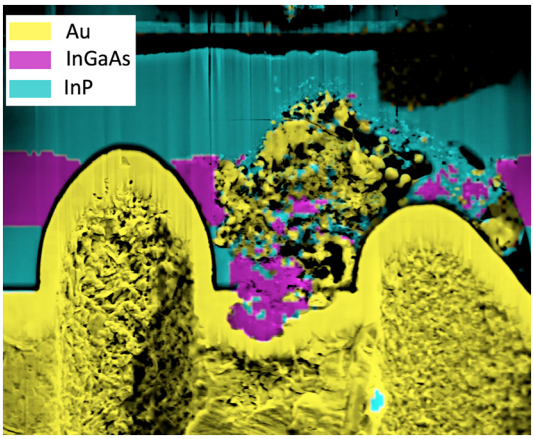

Fig. 7. EDS analysis of part of the active area of the QCL after cross-sections done by FIB.

of gold from upper metal gold layer (Fig. 7). Such situation is known to take place in semiconductor lasers, as metals from degraded electrodes or solder electromigrate inside the chip. This phenomenon is enhanced by current injection (electric field) and temperature.

However, it should be emphasized that the reason for the explosion and melting of active area resulting from overheating is not started in the internal part of the device as a result of low heat dissipation, but rather stems from the external factor - bad adhesion of gold to the semiconductor. This problem of poor adhesion in the initial phase of electrooptic and thermal tests, led to an increase in the threshold current caused by the creation of an additional channel for current flow. During thermal measurements with increased thermal load, the problem of bad gold contact became apparent. The increase local temperature caused by the lack of good thermal contact, led to destruction of metal layers on the upper laser surface, consequently leading to the damage of the whole device.

4. Conclusions

In this paper, we have presented and analyzed external degradation type of failure of the QCLs, associated with the damage of the top electrode. It is shown, how fabrication faults, identified in selected batches of devices, translate into degradation of device. We have registered temperature distributions and electrical characteristics of the device during the degradation process. Results show that the damage visible in AR does not necessarily stem from the fact of overheating resulting from high current flowing through active region during operation. We have observed that poor adhesion of dielectric away from the active regions itself, can lead to extensive thermal degradation of devices. The processes of electromigration of metals (i.e. gold) of top electrode are strongly enhanced by increased temperature (overheating) and high gradient of electric field.

Acknowledgement

The authors acknowledge contribution of M. Badura, B. Ściana and M. Tłaczała from Faculty of Microsystem Electronics and Photonics, Wrocław University of Science and Technology in MOVPE growth of InP waveguide layers.

This work was partially financially supported by the National Centre for Research and Development (NCBR) grant no. TECHMATSTRATEG1/347510/15/NCBR/2018 (SENSE) and National Science Center (NCN) under projects no. 2015/17/B/ST7/04015 (OPUS).

References

[1] V.S. Bagaev, Yu.N. Berozashvili, S. Ivanov, B.D. Kopylovski, Yu.N. Korolov, Pribory a Tekhnika Eksperimenta, 4 (1966), p. 185.
[2] D.P. Cooper, C.H. Gooch, R.J. Sherwell, Internal self-damage of gallium arsenide lasers, IEEE J. Quantum Electron. 2 (8) (1966) 329.
[3] H. Kressel, Observations concerning self-damage in GaAs injection lasers, IEEE J. Quantum Electron. 4 (1968) 176.
[4] J. Faist, F. Capasso, D.L. Sivco, C. Sirtori, C. Hutchinson, A.Y. Cho, Quantum cascade lasers, Science 264 (1994) 553.
[5] C. Gmachl, F. Capasso, D.L. Sivco, A.L. Cho, Recent progress in quantum cascade lasers and applications, Rep. Prog. Phys. 64 (2001) 1533.
[6] Y. Bai, N. Bandyopadhyay, S. Tsao, S. Slivken, M. Razeghi, Room temperature quantum cascade lasers with 27% wall plug efficiency, Appl. Phys. Lett. 98 (2011) 181102.
[7] M. Beck, D. Hofstetter, T. Aellen, J. Faist, U. Oesterle, M. Ilegems, E. Gini, H. Melchior, Continuous wave operation of a mid-infrared semiconductor laser at room temperature, Science 295 (2002) 301.
[8] M.J. Süess, R. Peretti, Y. Liang, J.M. Wolf, Ch. Bonzon, B. Hinkov, S. Nida, P. Jouy, W. Metaferia, S. Lourdudoss, M. Beck, J. Faist, Advanced fabrication of single-mode and multi-wavelength MIR-QCLs, Photonics 3 (2) (2016) 26.
[9] Y. Bai, S. Slivken, Q.Y. Lu, N. Bandyopadhyay, M. Razeghi, Angled cavity broad area quantum cascade lasers, Appl. Phys. Lett. 101 (2012) 081106.
[10] F. Xie, H. Nguyen, H. Leblanc, L. Hughes, J. Wang, J. Wen, D.J. Miller, K. Lascola, Long term reliability study and life time model of quantum cascade lasers, Appl. Phys. Lett. 109 (2016) 121111.
[11] Y. Sin, Z.Z. Lingley, M. Brodie, N. Presser, S.C. Moss, J. Kirch, C. Chang, C. Boyle, L. Mawst, D. Botez, D. Lindberg, T. Earles, Destructive physical analysis of degraded

quantum cascade lasers, Proc. SPIE 9382 (2015) 93821P.
[12] Q. Zhang, F.Q. Liu, W. Zhang, Q. Lu, L. Wang, L. Li, Z. Wang, Thermal induced facet destructive feature of quantum cascade lasers, Appl. Phys. Lett. 96 (2010) 141117.
[13] M. Fukuda, Reliability and Degradation of Semiconductor Lasers and LEDs, Artech House, Boston/London, 2001.
[14] M. Hempel, J.W. Tomm, F. La Mattina, I. Ratschinski, M. Schade, I. Shorubalko, M. Stiefel, H.S. Leipner, F.M. Kießling, T. Elsaesser, Microscopic origins of catastrophic optical damage in diode lasers, IEEE J. Sel. Top. Quantum Electron. 19 (4) (2013) 1500508.
[15] P.G. Eliseev, Optical strength of semiconductor laser materials, Prog. Quantum Electron. 20 (1996) 1.
[16] C.A. Evans, V.D. Jovanovic, D. Indjin, Z. Ikonic, P. Harrison, Investigation of thermal effects in quantum-cascade lasers, IEEE *J. Quantum Electron.* 42 (2006) 857.
[17] K. Pierściński, D. Pierścińska, K. Kosiel, A. Szerling, M. Bugajski, Influence of operating conditions on quantum cascade laser temperature, J. Electron. Mater. 39 (2010) 630.
[18] K. Pierściński, D. Pierścińska, M. Iwińska, K. Kosiel, A. Szerling, P. Karbownik, M. Bugajski, Experimental analysis of thermal properties of AlGaAs/GaAs quantum cascade lasers, Proc. SPIE 8432 (2012) 84320.
[19] D. Pierścińska, K. Pierściński, P. Gutowski, M. Badura, G. Sobczak, O. Serebrennikova, B. Ściana, M. Tłaczała, M. Bugajski, Heat dissipation schemes in AlInAs/InGaAs/InP quantum cascade lasers monitored by CCD thermoreflectance, Photonics 4 (2017) 47.
[20] P. Gutowski, I. Sankowska, P. Karbownik, D. Pierścińska, O. Serebrennikova, M. Morawiec, E. Pruszyńska-Karbownik, K. Gołaszewska-Malec, K. Pierściński, J. Muszalski, M. Bugajski, MBE growth of strain-compensated InGaAs/InAlAs/InP quantum cascade lasers, J. *Cryst. Growth* 466 (2017) 22.
[21] D. Pierścińska, K. Pierściński, M. Płuska, G. Sobczak, A. Kuźmicz, P. Gutowski, M. Bugajski, Temperature induced degradation mechanisms of AlInAs/InGaAs/InP quantum cascade lasers, Mater. Res. Express 5 (1) (2018) 016204.
[22] D. Pierścińska, K. Pierściński, M. Iwińska, K. Kosiel, A. Szerling, P. Karbownik, M. Bugajski, Electrical and optical characterisation of mid-IR GaAs/AlGaAs quantum cascade lasers, Proc. SPIE 8432 (2012) 84321S.
[23] P.W. Epperlein, Micro-temperature measurements on semiconductor laser mirrors by reflectance modulation: a newly developed technique for laser characterization, Jpn. J. Appl. Phys. Part 1 32 (1993) 5514.
[24] K. Pierściński, D. Pierścińska, M. Iwińska, K. Kosiel, A. Szerling, P. Karbownik, M. Bugajski, Investigation of thermal properties of mid-infrared AlGaAs/GaAs quantum cascade lasers, J. Appl. Phys. 112 (4) (2012) 043112.
[25] D. Pierścińska, K. Pierściński, M. Morawiec, P. Karbownik, P. Gutowski, M. Bugajski, CCD thermoreflectance spectroscopy as a tool for thermal characterization of quantum cascade lasers, Semicond. Sci. Technol. 31 (2016) 115006.
[26] D. Pierścińska, Thermoreflectance spectroscopy—analysis of thermal processes in semiconductor lasers, J. Phys. D. Appl. Phys. 51 (2018) 013001.